Mathematical Biology and Bioinformatics
2023. V. 18. № S. P. t54–t72. doi: 10.17537/2023.18.t54

Translation of the original article
Trusov P.V. et al. Mathematical Biology and Bioinformatics. 2015;10(1):34–53.
doi: 10.17537/2015.10.34

========== TRANSLATIONS OF PUBLISHED ARTICLES ==========

Flow in Antroduodenal Part of Digestive Tract: Mathematical Model and Some Results

Trusov P.V.[1,2], Zaitseva N.V.[1], Kamaltdinov M.R.[*1,2]

[1]*Federal Scientific Center for Medical and Preventive Health Risk Management Technologies, Perm, Russia*
[2]*Perm National Research Polytechnic University, Perm, Russia*

Abstract. A submodel of the digestive system is developed within the framework of multilevel model predicting the evolution of human functional disorders under environment influence. The article is dedicated to some problems associated with the submodel of food flow in the stomach. Materials in details is devoted to the reconstruction algorithm of 3D form andtroduodenal part of the digestive tract, based on ultrasonography results, and to the algorithm of the mesh node displacement caused by the antral contraction wave propagation and the pyloric sphincter motor activity. 3D form obtained and mesh configuration changing algorithm translated to program code are used for the flow calculation in antroduodenal part of the tract. Flow characteristics of one/two phased medium with opened/closed pyloric sphincter are analyzed considering functional disorders of the stomach motility; results are compared with 2D case. Further development ways of the stomach submodel and the digestive system model are noted: considering functional disorders of the pyloric sphincter, periodicity disorders of the antral contraction wave propagation in the stomach, processes of the digestive juice secretion, absorption of substances into the circulatory system.

Key words: *digestive system, functional disorders, peristaltic waves, flow in stomach, pyloric sphincter.*

INTRODUCTION

Health assessment and prediction of life expectancy are priority tasks to be solved within various spheres of scientific knowledge and applied subjects, from gerontology to planning health protection activities on the federal and regional levels. It is noteworthy that if experimental approaches allow only the current estimation of health or any physiological disorders, life expectancy prediction traditionally uses models based on statistical and probabilistic approaches. Several statistical theories describe natural accumulation of damage in the body resulting in death; among them, we can mention theories of natural ageing based on analyzing sex- and age-specific population mortality [1–3] and theories of failure (reliability) [4, 5]. The aforementioned approaches are widespread in epidemiology and demographics [6, 7] although they do not consider mechanisms of disorders and mutual influence exerted by various processes on each other. This is probably due to absence of a unified concept on ageing mechanisms in the expert community. For example, the homeostatic model developed by V.N. Novosel'tsev [8, 9] describes ageing as a process associated with oxidative damage accumulating in the human body over time. Other authors pay attention to neuro-immune-endocrine ageing mechanisms [10] etc. A substantial number

[*]kmr@fcrisk.ru

of models do not consider environmental factors and their contributions to damage accumulation in the body. Meanwhile, negative effects produced on the body by heterogeneous environmental factors shorten average life expectancy down to 70–75 years whereas the species-specific limit of human life expectancy is estimated as equal to 110–120 years [11].

If we wish to consider environmental exposures, we cannot fail to notice several advantages of mathematical models. They provide easy management of factors (inclusion/exclusion), allow assessing contributions of factors to health disorders, and give an opportunity to model with life- and health-threatening boundary values of factors, which are impossible to be used in experiments. Several approaches that consider environmental factors deserve some attention; they are statistical risk load models that describe an additional component in intensity of mortality [12] and the body lifecycle model [13, 14]. Analyzed objects are complex and physiological processes typically have wide spatial and time scales. This calls for using multi-level approaches to investigating them.

We have been working as a research team on developing a multi-level mathematical model [15, 16]. It aims to assess influence of environmental factors on human health; another goal is to predict functional disorders in the human body developing under exposure to chemical, physical, social, and other factors. At this stage in the research, we have developed the structure, basic concepts and definitions of the mathematical model at the macro-level; meso-level models describing the digestive, respiratory, cardiovascular, immune, and endocrine systems are being developed [17]. It is necessary to establish kinetic relationships for chemicals introduced into the body with foods and drinking water. To do that, a meso-level sub-model of the digestive system is required, in particular, to describe the gastrointestinal tract (GIT). The digestive system is closely connected with other organs and systems such as the circulatory, nervous and endocrine system. Chemicals introduced through the GIT are absorbed into the circulatory system and spread throughout the whole body; on the other hand, the digestive organs are provided with all the substances necessary for secretion and nutrition from blood that flows through them. Blood brings not only benign substances but also chemicals that can produce negative effects on the digestive organs. These chemicals are entered into the body through other systems (the respiratory system, for example). Digestive processes are managed by neuro-humoral mechanisms with their activity also depending on properties of a mixture in the gastrointestinal tract (feedback). In future it may become necessary to develop some models at the micro-level to consider secretion, absorption, hormonal regulation etc. at the cellular level or even below.

Experimental studies are a conventional way to investigate physiology of digestive processes. They are divided into experiments *in vivo* when digestive processes are examined in a live organism after food consumption and experiments *in vitro* that involve using experimental equipment to simulate digestive processes.

Magnetic resonance imaging (MRI) is one of the most widespread methods to examine the GIT activity *in vivo*. It provides high-resolution images of internal organs, in different cross-sections and with a short time interval. MRI results are used to estimate the GIT motor activity and the rate of stomach evacuation [18, 19]. The major disadvantage of the method is the necessity to use expensive equipment; besides, an examination is made when a patient is lying and food distribution in the GIT is different in this case as opposed to sitting or standing [20]. Radionuclide scanning is a method able to visualize the digestive process. An image is created due to radiation of radioactive isotopes consumed with food. This method is used to identify how food particles are distributed in the GIT in dynamics and to estimate stomach evacuation [21]. Radionuclide scanning also has a major drawback, which is the use of radioactive chemicals that can affect health. Ultrasound (US) results are used to build a geometrical shape of organs and assess the GIT motor activity [22, 23]. All the analyzed visualization techniques, excluding intracavitary US, do not involve penetration of any

sensors or probes into the body that can distort experimental results. This is obviously an advantage.

To measure local intracavitary pressure in the GIT directly, alien objects are usually introduced into the body. They can be different vessels, sensors, or catheters. Gastrointestinal manometry with a multi-channel water-perfusion catheter is the most widespread method [24, 25]. It is noteworthy that despite all the existing drawbacks associated with measurement precision no alternative approach to measuring the GIT pressure is available at the moment [26]. Electrogastroenterography, an experimental method, was applied to estimate the motor-evacuation function by registering electric signals coming from the digestive organs. It is based on a relationship between the electric GIT activity and its motor activity [27–29]. The secretory function of the stomach is estimated with pH metry, direct measurement of acidity in the GIT [30]. This procedure can be accomplished together with endoscopy, visual assessment of the gastric mucosa with an optical system introduced through the mouth and esophagus [31]. Most aforementioned approaches *in vivo* take a lot of time to prepare and conduct an experiment and require highly qualified experts to accomplish them.

Experiments *in vitro* save a lot of time and material resources as opposed to *in vivo* studies. A widely used way to simulate processes in the GIT involves subsequent adding of substances and enzymes corresponding to different stages in digestion into a vial with food; in some cases, its contents are mixed periodically [32], and sometimes peristaltic waves are imitated [33]. As a rule, the method is applied to estimate how rapidly medications and food particles are decomposed down to elements that can be assimilated [34–36]. Devices that are more complex consist of several chambers corresponding to different GIT section [37] where secretion and peristaltic motility are managed by a computer [38]. Some up-to-date devices not only simulate the chemical structure of the digestive juice but also imitate effects of additional mechanical forces that replace effects produced by the motor activity on a food sample [39, 40]. A major disadvantage of experiments *in vitro* is difficulty in creating a real geometric shape of the GIT with its moving boundaries.

Improvement of experimental equipment and methods for medical image processing has facilitated active development of mathematical modeling in the sphere over the last two decades. In particular, we can mention research works with their focus on creating mathematical models of digestive processes [41]. Mathematic modeling has a major advantage since it saves time and resources. In a mathematical model, you can change parameters of analyzed processes by including individual shapes and sizes of analyzed organs as well as functional disorders in them until their complete failure occurs. You can analyze effects produced by specific factors or their combinations or simulate oral entry of chemicals in health-threatening doses unacceptable for full-scale experiments. It is noteworthy that development stage requires experimental data for proper identification and verification of model parameters.

Kinetic chamber models are widely used to estimate concentrations of various substances in the circulatory, digestive, and other systems in the human body [42, 43]. Unfortunately, they do not allow tracing how special characteristics of various processes change over time since they are generally based on a system of ordinary differential equations with time as a single independent variable. Given that, it seems advisable to estimate oral entry of chemicals by continuum mechanics methods (hydrodynamics of heterogeneous media) and using partial differential equations describing spatial-temporal regularities. An advantage of this approach is its high informative value; it gives an opportunity to model basic digestive processes including absorption and secretion (diffusion processes), tract wall motility, food grinding and dissolving, and biochemical reactions in the gastrointestinal tract cavity.

Although approaches to numeric modeling of flows in various GIT sections (the esophagus, stomach, and intestines) have started to develop over the last decades, the number of created 3D-models is still rather limited [44–46]. Models that simulate the flow in the antroduodenal section of the GIT are the most interesting as regards mechanics [47, 48] since

effects of stirring and homogenizing a food mixture are the most apparent in it due to intensive peristalsis [49]. Modeling results show that a liquid flow is reverse to the direction of peristaltic waves and that circulating flows occur between peaks of two neighboring waves [50, 51] making it easier for stomach contents to be mixed thoroughly. As a rule, the existing models do not consider evacuation from the stomach into the intestines and the pyloric sphincter motility; they mostly analyze a flow of one-phase Newtonian liquid. Any research in this area requires further development of such models so that they cover all the aforementioned basic digestive processes as well as neuro-endocrine regulation and functional disorders of relevant organs.

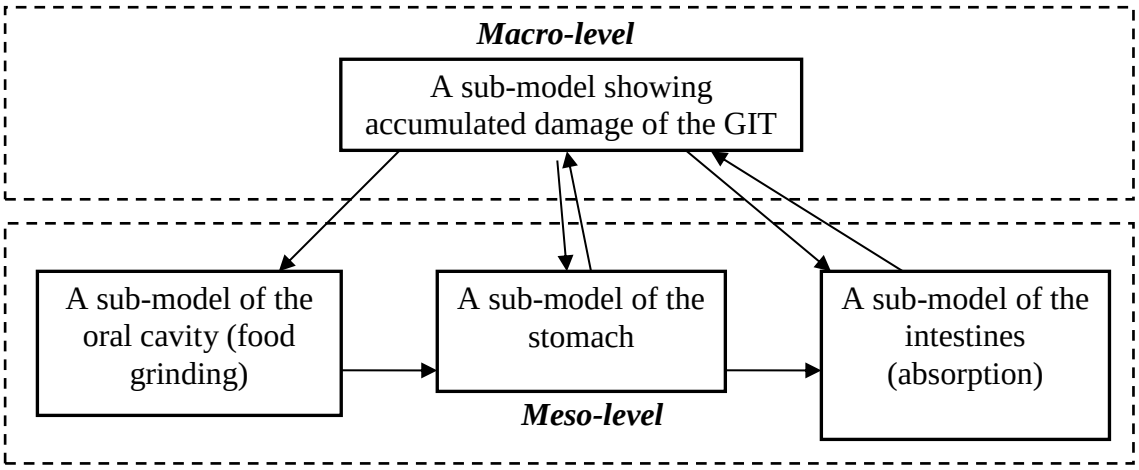

Fig. 1. The relation between macro-level and meso-level sub-models.

At present, the meso-level model of the digestive system has basic concepts and definitions and its conceptual statement has been developed [52]; three sub-models are created according to the GIT sections, the oral cavity, stomach, and intestines (Fig. 1).

On the macro-level, an individual human body is considered a system that consists of a finite number of interrelated organs. Interactions between different organs are accomplished due to substance and energy streams reflecting, among other things, environmental exposures. To describe functional disorders of the j-th organ at the macro-level, we introduce damage $D_j(t)$ as a time-(age)-dependent parameter t, $D_j(t) \in [0, 1]$; if $D_j = 0$, it means proper (ideal) functioning; if $D_j = 1$, it means an organ (a system) is unable to perform its functions. The human body as a biological system tends to accumulate functional disorders over time; they become apparent as diseases. Changes in damage of human organs and systems occur due to effects produced by several mechanisms; the most significant ones are natural ageing, organ self-recovery, accumulation of damage due to environmental exposures beyond their safe levels, and recovery of functions due to treatment. The rate of changes in damage $D_j(t)$ of the j-th organ (system) is assumed to be determined by the sum of all rates of damage occurring due to all the aforementioned mechanisms.

When considering the GIT, we can identify two mechanisms of damage accumulation under environmental exposures beyond their safe limits. They are direct irritating effects produced on the tract walls by chemicals occurring in the GIT cavity and effects produced by chemicals that are contained in blood flowing through the GIT organs. Intensity of these effects is determined as per chemical levels in the near-wall layer of the GIT organs and blood accordingly.

The level of damage helps identify associated functionality of an organ (system) $F_j(t)$, which we consider an ability of the j-th organ to perform its functions. In the GIT, these functions are motility, secretion, and absorption. A relationship between functionality and damage can be written, for example, as $F_j(t) = (1 - D_j(t))^{n_j}$, $n_j \in R \geq 1$. Functional disorders

can lead to changes in chemical concentrations in blood and the GIT cavity and the rate of damage accumulation will also change (a feedback).

Since the tasks to be solved are complex and multidimensional, this article concentrates on only a fragment of a meso-level model that describes the digestive system. This is a sub-model of flows in the stomach, namely, in the antroduodenal section of the GIT. This model is per se the core of the meso-level model describing the digestive system. Besides, given all the above-stated, it seems interesting to create models of flows in the stomach even separately from other sub-models. The meso-level model of the digestive system will have its complete prediction capacity as regards functional disorders in the body only after all the relevant sub-models have been created and all the relations between them have been properly identified. Within this study, we consider only damage of the stomach $D(t)$ and associated functionality $F(t) = 1 - D(t)$ (therefore no indexes are provided here and below in the text).

At the previous stage in developing the stomach sub-model, we computed the flow in the antrum considering motor functionality in the two-dimensional statement and outlined how to develop the sub-model in future by switching to a three-dimensional task and considering the pyloric sphincter motility [52]. Therefore, this article provides a detailed description of an algorithm applied to reconstruct a simplified three-dimensional shape of the antroduodenal section in the GIT as per US results as well as an algorithm applied to compute how nodes in the computation mesh would shift under exposure to a peristaltic wave in the antrum and the pyloric sphincter motility. The obtained three-dimensional shape and the coded algorithm of changes in the mesh configuration are applied to compute the flow in the antroduodenal section of the GIT. We analyze a flow of one/two-phase medium with the opened/closed pyloric opening and compare the results with the two-dimensional statement.

MATHEMATICAL STATEMENT OF THE TASK RELATED TO DESCRIBING FLOWS IN THE STOMACH

We consider a flow of a two-phase mixture. The first phase is water and the second phase is liquid food particles with increased density. Since there is no inter-phase exchange, mass conservation equations can be written for each phase as [53]:

$$\frac{\partial(\alpha_1\rho_1)}{\partial t} + \nabla\cdot(\alpha_1\rho_1\mathbf{v}_1) = 0, \tag{1}$$

$$\frac{\partial(\alpha_2\rho_2)}{\partial t} + \nabla\cdot(\alpha_2\rho_2\mathbf{v}_2) = 0, \tag{2}$$

$$\alpha_1 + \alpha_2 = 1. \tag{3}$$

where α_1, α_2 are volume fractions of the first and second phase, ρ_1, ρ_2 are phase densities, $\mathbf{v}_1$, $\mathbf{v}_2$ are phase velocities.

We accept a hypothesis that phase pressures are equal and the power of interphase interaction is proportionate to the difference between the velocities of the interacting phases. In this case, the system of impulse conservation equations for the flow of liquid incompressible phases is written as:

$$\frac{\partial}{\partial t}(\alpha_1\rho_1\mathbf{v}_1) + \nabla\cdot(\alpha_1\rho_1\mathbf{v}_1\mathbf{v}_1) = -\alpha_1\nabla p + \nabla\cdot\boldsymbol{\tau}_1 + \alpha_1\rho_1\mathbf{g} + K_{21}(\mathbf{v}_2 - \mathbf{v}_1), \tag{4}$$

$$\frac{\partial}{\partial t}(\alpha_2\rho_2\mathbf{v}_2) + \nabla\cdot(\alpha_2\rho_2\mathbf{v}_2\mathbf{v}_2) = -\alpha_2\nabla p + \nabla\cdot\boldsymbol{\tau}_2 + \alpha_2\rho_2\mathbf{g} + K_{12}(\mathbf{v}_1 - \mathbf{v}_2), \tag{5}$$

$$\boldsymbol{\tau}_1 = \alpha_1\eta_1(\nabla\mathbf{v}_1 + (\nabla\mathbf{v}_1)^T), \tag{6}$$

$$\boldsymbol{\tau}_2 = \alpha_2\eta_2(\nabla\mathbf{v}_2 + (\nabla\mathbf{v}_2)^T), \tag{7}$$

Mathematical Biology and Bioinformatics. 2023. V. 18. № S. doi: 10.17537/2023.18.t54

where p is the mixture pressure, η_1, η_2 are shear viscosities, $\mathbf{g}$ is the vector that describes effects of mass forces, $\boldsymbol{\tau}_1$, $\boldsymbol{\tau}_2$ is the stress tensor, $\nabla\cdot$ is divergence, $\mathbf{v}_1\mathbf{v}_1$, $\mathbf{v}_2\mathbf{v}_2$ is the dyadic product of the velocity vectors, $(\cdot)^T$ is the transposition sign, K_{12} is the coefficient of interphase interaction; for spherical particles at $\mathrm{Re}_{ji} \le 1000$ (liquid phases have low velocity), it can be written as [54]:

$$K_{12} = K_{21} = \frac{18\alpha_1\alpha_2\eta_1}{d_2^2}(1+0.15\,\mathrm{Re}_{12}^{0.687}), \tag{8}$$

where $\mathrm{Re}_{12} = \mathrm{Re}_{21} = \rho_1|\mathbf{v}_2 - \mathbf{v}_1|d_2/\eta_1$, d_2 is the diameter of the second phase particles.

Functional disorders of the stomach motility are suggested to be considered when setting amplitude of antral peristaltic waves; this can be written as $A(F,t) = A(t)\cdot F(t)$, where $A(t)$ is the value of the wave amplitude at the moment t in case functional disorders are absent. Therefore, functional disorders of the stomach motility are assumed to have no influence on the velocity of the wave propagation (it depends on the nervous system functionality, namely, the rate of nervous impulse transfer) and to exert impacts only on intensity of the circular muscle layer contractions (muscle weakness).

Although the methods for reconstructing a realistic three-dimensional shape of organs using two-dimensional MRI and US images are well developed [55–59], we plan to use a bit simplified algorithm for reconstructing a three-dimensional shape of the antroduodenal section in the GIT. This algorithm provides analytical description of the organ configuration necessary for setting the law of peristaltic wave propagation.

Kinematic boundary conditions are set on the walls of the GIT antroduodenal section considering peristalsis:

$$\mathbf{v}(t,\mathbf{x}_w) = \mathrm{d}\mathbf{x}_w/\mathrm{d}t, \tag{9}$$

where $\mathbf{x}_w$ is the displacement vector for the material point of the wall of the GIT antroduodenal section. The zero pressure gradient $\nabla p = 0$ is set at the other boundaries of the analyzed area (input/output cross-sections).

The suggested algorithm is described on the example of the GIT antroduodenal section, which has average statistical geometric properties (sizes and shape). In future, we plan to introduce some parameters in the model that will allow changing the stomach shape depending on individual peculiarities.

THE ALGORITHM FOR RECONSTRUCTING A THREE-DIMENSIONAL SHAPE OF THE GIT ANTRODUODENAL SECTION

The published reports about numeric experiments [50] show that boundary conditions have substantial influence on solution results. Moreover, changes in some parameters of the peristaltic activity (for example, contraction amplitude), other conditions being equal, can produce quantitatively and qualitatively different solutions [51]. Given that, it is very important to set boundary conditions correctly, both for normal functioning and for functional disorders. Geometric parameters of the stomach and motility parameters vary significantly between individuals; the latter also depend on consumed food, a digestion phase and functional disorders. Bearing this in mind, it seems advisable to reconstruct a three-dimensional shape of the GIT antroduodenal section relying on results of a real experiment. Wave characteristics should be identified in the same experiment (associated with the geometric shape of the stomach at a certain time moment).

1) US provided images of the stomach (a body was in the vertical position) in planes parallel to two basic anatomic planes, the horizontal one (parallel to the ground level) and the

median one (divides the human body into two symmetrical halves). The stomach sizes were estimated at a first approximation and the reference points were identified on the lesser and greater curvature of the antrum in the third basic (frontal) anatomic cross-section (frontal cross-section coincides with the *xy* plane).

2) The central line in the antrum is identified as the median line between the curves approximating the lesser and greater curvature. It is located in the *xy* plane and approximated with the 6th degree polynomial (Fig. 2):

$$y(x) = 25625.919x^6 + 17005.606x^5 - 3256.476x^4 + \\ +197.116x^3 + 4.208x^2 - 0.75198x + 0.02541, \quad (10)$$

where $x \in [0.007942; 0.0948]$ m.

3) The next stage involves approximating cross-sections of the three-dimensional stomach surface with ellipses; their centers lie on the central line and ellipses are located in the normal plane (the normal plane to the spatial curve is the plane normal to the tangent straight line and coming through the point of tangent) to the central line. The greater ellipse semi-axis $r_1(x)$ is located in the plane *xy*, the lesser semi-axis $r_2(x)$ is normal to the plane *xy* (parallel to the *z* axis), the ellipse with its center at the point (x_c, $y(x_c)$, 0) is described by:

$$\begin{cases} \dfrac{[(x-x_c)\sin(\text{arctg}(f'(x_c)) + (y-y_c)\cos(\text{arctg}(f'(x_c))]^2}{r_1^2(x_c)} + \dfrac{z^2}{r_2^2(x_c)} = 1, \\ \cos(\text{arctg}(f'(x_c)) \cdot (x-x_c) + \sin(\text{arctg}(f'(x_c)) \cdot (y-y_c) = 0. \end{cases} \quad (11)$$

Here $y(x_c)$ is the value of the function (10) at the point x_c, $f'(x_c)$ is the value of the function (10) derivative at the point x_c, the relationship between the greater ellipse semi-axis and the coordinate *x* in the antrum is given by the quadratic function $r_1(x) = 1.234x^2 + 0.112x + 0.00942$, the $r_2(x)$ to $r_1(x)$ ratio in the stomach antrum and pyloric opening is assumed to be constant and equal to 0.613 (the estimation is based on US results).

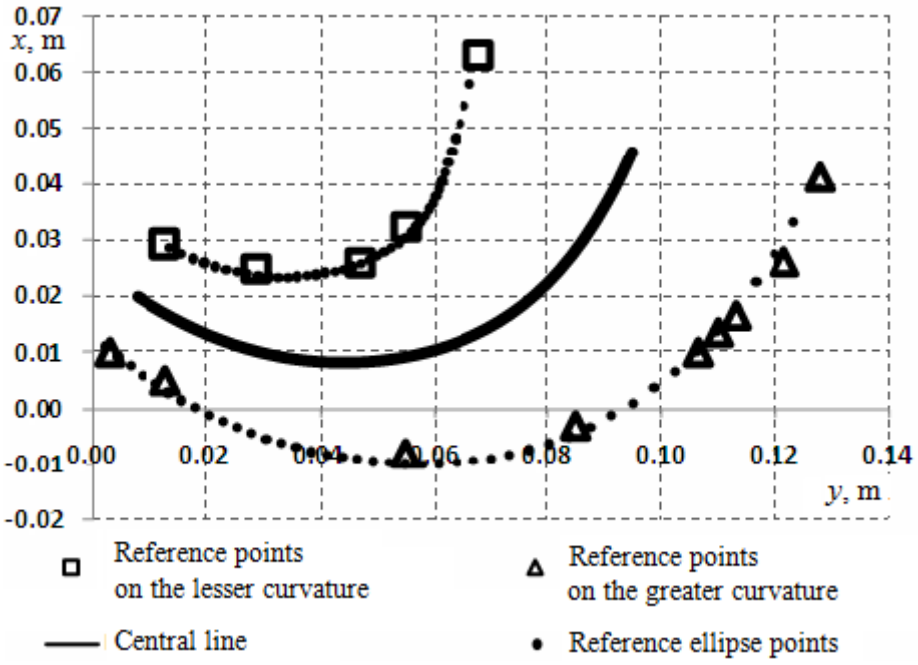

Fig. 2. The central line of the antrum in the plane *xy*.

It is noteworthy that the suggested algorithm has certain limitations in its application since unique properties of the stomach structure can make areas intersect inside the created ellipses.

In this case, it is necessary to develop other approaches to reconstructing the stomach shape and setting peristaltic waves.

4) The computed coordinates of the reference ellipses are exported into the *Ansys Design Modeler*, and the three-dimensional surface is approximated with the *skin/loft* tool (Fig. 3). The central line of the pyloric opening area is identified as per the relationship (10) (where $x \in [-0.012057; 0.007942]$ m), the greater ellipse semi-axis in the r_1 segment is equal to

$$r_1 = r_{1p} - \alpha \cdot r_{1p} \cdot \frac{1 + \sin\left(\pi(\lambda_p - \rho_1)/2\lambda_p\right)}{2}, \quad \text{at } \rho_1 \le \lambda_p, \tag{12}$$

where $r_{1p} = 0.0102586$ m is the greater ellipse semi-axis at the entry zones to the stomach and intestines, $\lambda_p = 0.012$ m is the distance from the most narrow part of the pyloric opening area to the stomach area, ρ_1 is the distance from the center of the ellipse with the greater semi-axis r_1 to the most narrow part of the area ($x = -0.002557$), $\alpha = 0.55$ when the sphincter is open, $\alpha = 0.95$ when the sphincter is closed, which corresponds to changes in the greater semi-axis of the pyloric opening in the most narrow elliptical cross-section between 0.00461 m and 0.00051 m. The complete sphincter closure is simulated with a lesser opening in order to provide existence of the solution to medium flow equations and stability of computations in the pyloric opening area. In future, we are going to introduce some additional parameters as well as criteria for them, which will manage the state of the sphincter (sufficient food grinding, the medium acidity, and the nervous system condition). The ratio between the lesser and greater semi-axes r_2 and r_1 in the pyloric opening area is assumed to be the same as in the stomach, equal to 0.613.

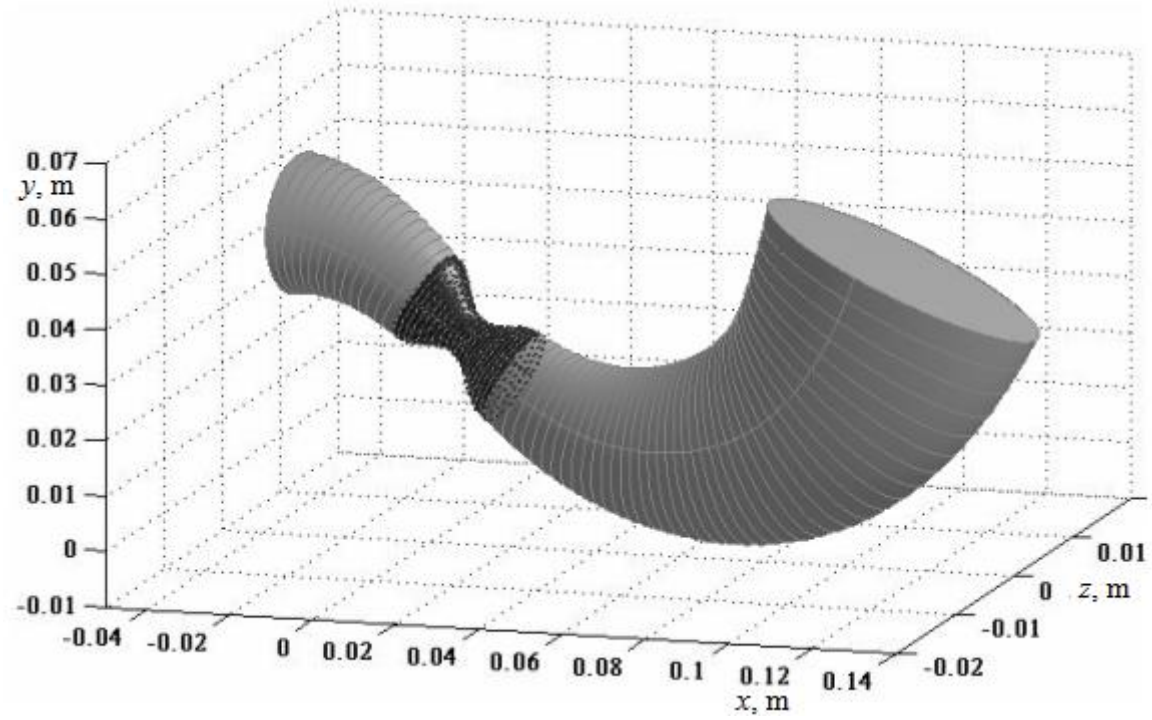

Fig. 3. Building up the surface of the stomach antroduodenal section (the colored segment is the pyloric opening area, the intestines are to the left of it and the antrum is to the right).

At a first approximation, the central line of the intestines is described by the quadratic dependence on the coordinate *x*:

$$y = -14.34x^2 - 1.207x + 0.022, \tag{13}$$

where $x \in [-0.04; -0.012057]$ m, the greater and lesser ellipse semi-axes r_1 and r_2 change linearly to the value of 0.014 m; therefore, the cross-section of the intestines takes on a round shape at the left boundary, which corresponds to data available in anatomic reference books.

5) A computation mesh is created in the *Ansys Meshing*; it consists of 717,953 tetragonal elements. The size of the surface element edge varies between $0.6 \cdot 10^{-3}$ m (in the areas close to the lesser curvature in the antrum and close to the pyloric opening) and $1.5 \cdot 10^{-3}$ m (in the areas close to the greater curvature in the antrum).

THE ALGORITHM FOR IDENTIFYING SHIFTS OF THE COMPUTATION MESH NODES

Wave propagation and the pyloric sphincter motility are simulated based on available literature data [50, 51] and US results. Several minutes after food consumption, contraction waves start to propagate in the antrum, that is, some areas (strips) in the circular muscle layer contract along the elliptic cross-section of the stomach. After contraction, an area of circular muscles relaxes and contraction waves move on to another area.

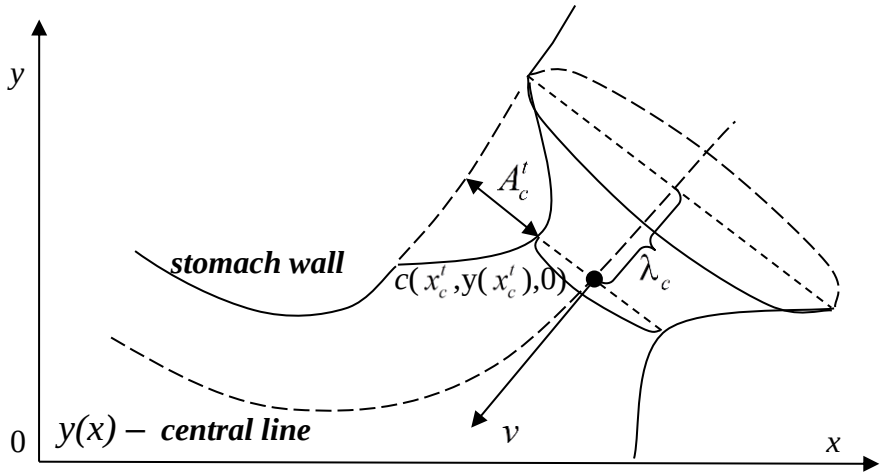

Fig. 4. Parameters of the contraction wave in the antrum**.**

The antral contraction wave is initiated in the elliptic cross-section with the center at the point $x = 0.088$ m and then moves to the pyloric opening with the velocity being $v = 2.2 \cdot 10^{-3}$ m/s, directed at a tangent to the central line, during 38 s. The point at the central line, which corresponds to the elliptic cross-section with the maximum contraction, is described as $c(x_c^t, y(x_c^t), 0)$. The baseline scenario has the following wave parameters (Fig. 4): a half of the wave width $\lambda_c = 0.01$ m is independent of time, the contraction amplitude A_c^t grows linearly during the first 12 s until it reaches 0.011 m provided there are no functional disorders ($A(t,c) = A_c^t = F(t) \cdot (t/12) \cdot 0.011\,\text{m}$); the amplitude remains constant at the time moment $t \in [12, 34]$ and goes down linearly to 0 at the time moment $t \in [34, 38]$. Waves are initiated with an interval equal to 18 s. The sphincter opens at $t \in [28, 30]$ and closes at $t \in [32, 34]$ (Fig. 5).

The computation mesh is reconstructed dynamically with *Dynamic Mesh* tools in the *Fluent* solver; they compute the location of internal nodes automatically based on the present configuration of the boundary element at each time moment [60]. Shifts of the boundary nodes during an antral contraction wave moves and the pyloric sphincter opens/closes are identified using a script (*User-Defined Function*) written in C. The script is a software implementation of a stage-by-stage procedure (the algorithm is described below). It is noteworthy that shifts of the boundary nodes occur only in the corresponding elliptical cross-section imitating circular muscle contractions.

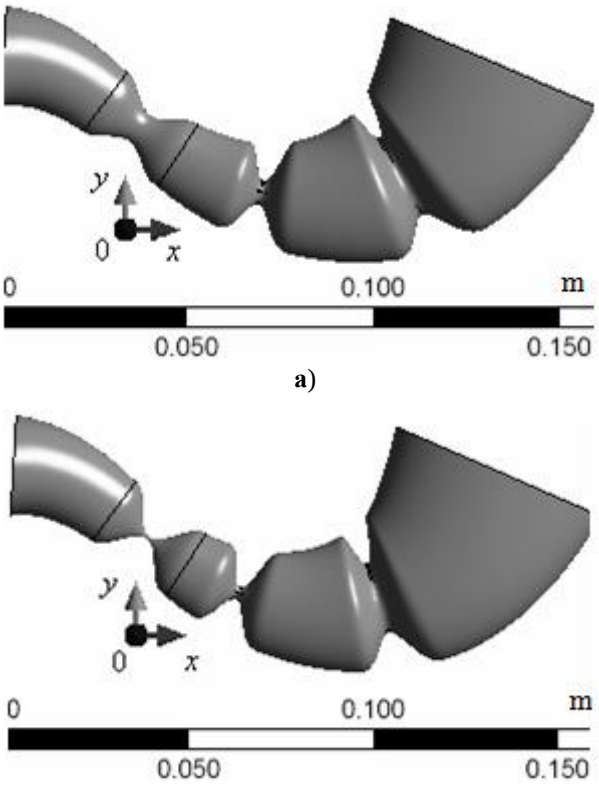

Fig. 5. Wave location in the antrum when **a**) the pyloric sphincter is open; **b**) the pyloric sphincter is closed.

We would like to consider the algorithm for identifying shifts of the boundary nodes in detail.

1) The coordinate of the point x_c^t at the central line is identified at the next computed moment of time by using the following relationship:

$$x_c^{t+1} = x_c^t - \Delta t \cdot \cos(\text{arctg}(y'(x_c^t))) \cdot \nu \,, \tag{14}$$

where $y'(x_c^t)$ is the derivative of the function (10) at the point x_c^t, Δt is a step in time. When deriving the equation (14), we assume the wave velocity v to be directed at a tangent to the central line.

2) Each boundary node in the computation mesh lies on the ellipse identified by the formula similar to the (11) in the initial configuration (with the center coordinates being $(x_{cnode}, y_{cnode}, 0)$) and shifts only with the normal plane to the central line. The ellipse center is identified based on the condition $\rho_{node} = \rho((x_{node}^t, y_{node}^t, z_{node}^t), (x_{cnode}, y_{cnode}, 0) \to \min$ (the perpendicular from the node to the central line), where $(x_{node}^t, y_{node}^t, z_{node}^t)$ are the node coordinates at a computed moment of time, $(x_{cnode}, y_{cnode}, 0)$ are the ellipse center coordinates, ρ_{node} is the distance between the node and the ellipse center (Fig. 6).

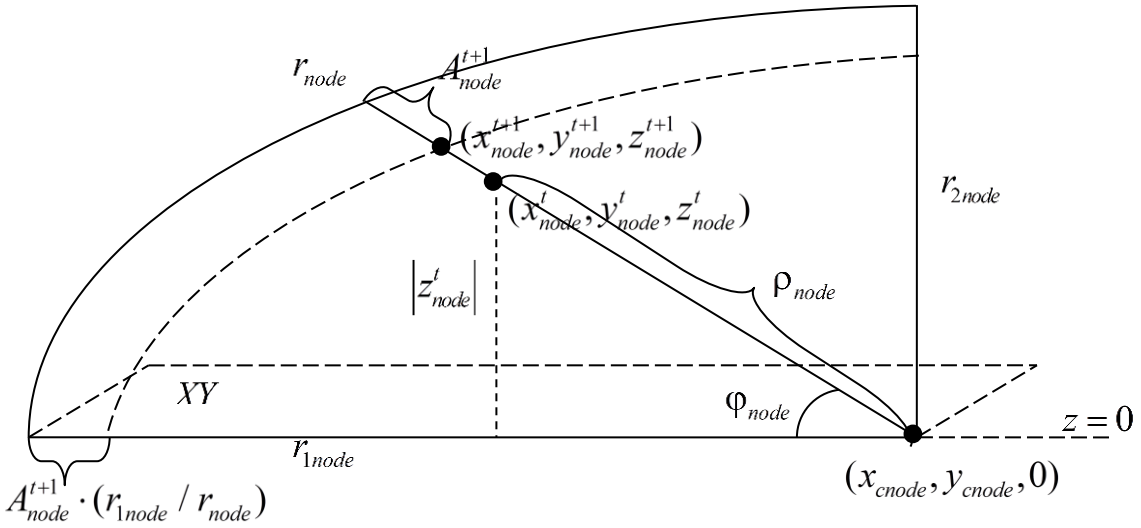

Fig. 6. The scheme illustrating the algorithm for defining shifts of the computation mesh nodes.

3) The greater semi-axis r_{1node} of the ellipse ocorresponding to a node in the computation mesh in the initial configuration is identified from the (11), the angle between the semi-axis r_{1node} and the perpendicular from the node to the central line is equal to:

$$\varphi_{node} = arctg\left(\frac{|z_{node}^{t}|}{\sqrt{(y_{node}^{t} - y_{cnode})^2 + (x_{node}^{t} - x_{cnode})^2}}\right). \quad (15)$$

The distance between the ellipse center and a node in the computation mesh in the initial configuration is equal to:

$$r_{node} = \frac{r_{1node} \cdot r_{2node}}{\sqrt{r_{2node}^2 \cos^2 \varphi_{node} + r_{1node}^2 \sin^2 \varphi_{node}}}, \quad (16)$$

where r_{1node} is the greater ellipse semi-axis in the initial configuration and r_{2node} is the lesser ellipse semi-axis in the initial configuration.

4) The location of the boundary node in the antrum at a computed moment of time is identified by a shift from its non-deformed state along the perpendicular to the central line using the following function:

$$A_{node}^{t+1} = (r_{node} / r_{1node}) \cdot A_c^{t+1} \cdot (1 + \sin(\pi \cdot \frac{\lambda_c - \rho_c}{2\lambda_c}))^2 / 2, \text{ at } \rho_c \le \lambda_c, \quad (17)$$

where A_{node}^{t+1} is a shift magnitude, $\rho_c = \rho((x_{cnode}, y_{cnode}, 0), (x_c^{t+1}, y_c^{t+1}, 0))$ is the distance between the ellipse center and the point $c(x_c^{t+1}, y(x_c^{t+1}), 0)$. Exponentiation of a multiplier with sinus (squaring in this case) provides smoothing at the wave peak. It is noteworthy that literature data and ultrasound results indicate it is possible to use functions with sinus when describing the peristaltic wave shape.

5) The coordinates of a new location of a node in the antrum wall are computed as per the following formulas:

$$x_{node}^{t+1} = x_{cnode} + (x_{node}^{t} - x_{cnode}) \cdot (r_{node} - A_{node}^{t+1}) / \rho_{node}, \quad (18)$$

$$y_{node}^{t+1} = y_{cnode} + (y_{node}^{t} - y_{cnode}) \cdot (r_{node} - A_{node}^{t+1}) / \rho_{node}, \quad (19)$$

$$z_{node}^{t+1} = z_{node}^{t} \cdot (r_{node} - A_{node}^{t+1}) / \rho_{node}. \quad (20)$$

Mathematical Biology and Bioinformatics. 2023. V. 18. № S. doi: 10.17537/2023.18.t54

6) The location of the boundary node in the pyloric opening area when the sphincter is open/closed at a computed moment of time is identified by a shift from its non-deformed state along the perpendicular to the central line by using the linear law from time depending on the values of the α parameter in the formula (12).

RESULTS

We have analyzed three different scenarios: a flow of a one-phase liquid without any functional disorders of motility; a flow of a one-phase liquid with functional disorders; a flow of a two-phase liquid with functional disorders. Besides, we have investigated what influence the pyloric sphincter has on these flows. According to the preset parameters, waves are periodical in the antroduodenal section of the stomach (with a period of 18 s); since it takes a wave 38 s to go through the antrum, we can observe two or three waves in the stomach at different time moments.

The inflow condition is set at the right and left boundaries, namely, the zero relative pressure. A condition is set at all the remaining boundaries of the computed area stating that they are impermeable and friction is absent. A time step remains constant over the whole analyzed period and equals 0.01 s.

In the first scenario, water is considered as a medium ($\rho = 1000$ kg/m^3; $\eta = 10^{-3}$ Pa·s). When the pyloric sphincter is closed ($t \le 28$ s), the flow character (Fig. 7) is consistent with previous results obtained for a two-dimensional task [52], with known literature data [50], and with results of three-dimension modeling, that does not consider evacuation into the intestines [44].

We observe how a flow zone occurs with its velocity reaching 0.031 m/s and directed oppositely to the velocity of peristaltic wave propagation; also, we can see areas with circulating flows between peaks of neighboring waves. When a peristaltic wave reaches the antrum middle, the pyloric sphincter opens, and as it remains open, the stomach contents are evacuated into the intestines at the velocity reaching 0.016 m/s. The flow velocity in the antrum drops to 0.019 m/s (Fig. 8).

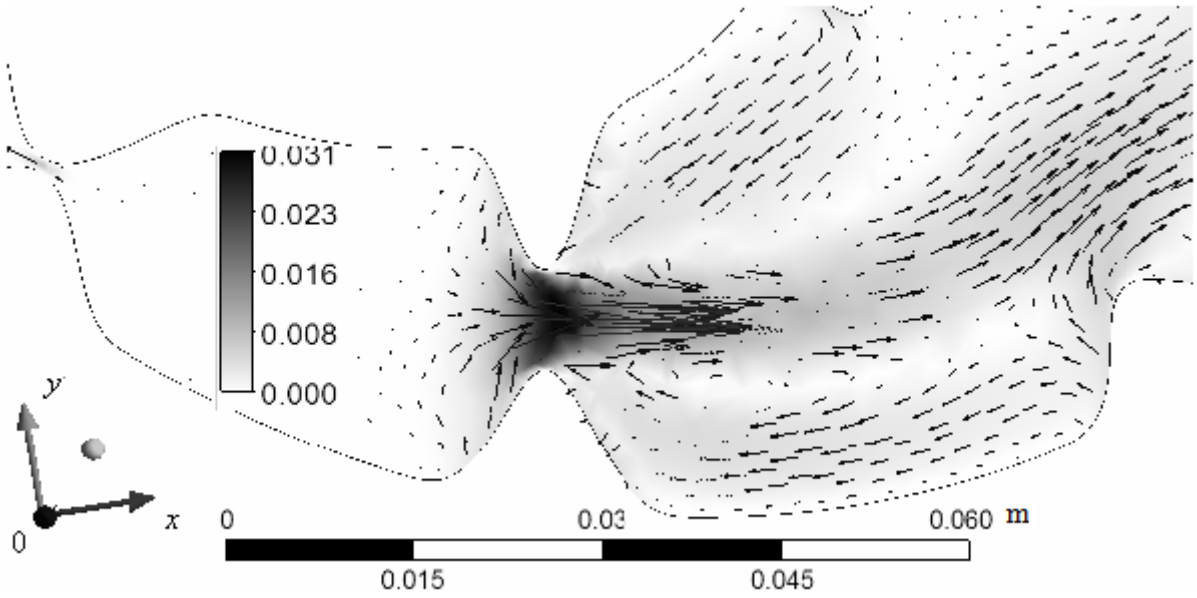

Fig. 7. The velocity field in the antrum when the pyloric sphincter is closed (t = 28 s), m/s.

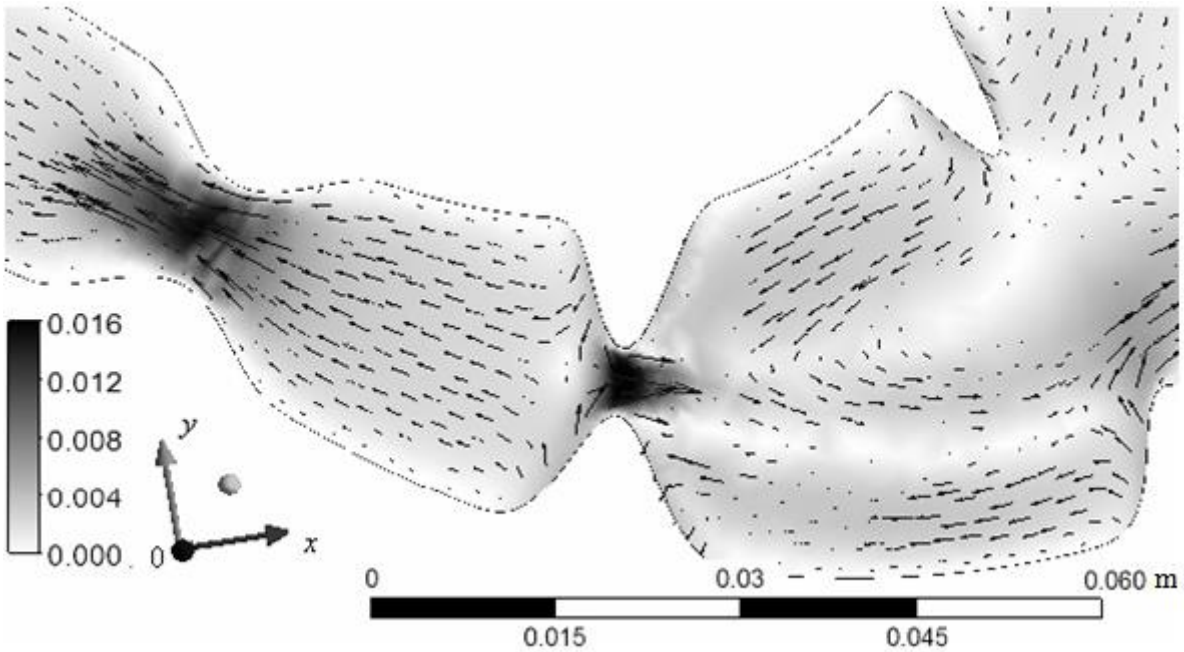

Fig. 8. The velocity field in the antroduodenal section of the stomach when the pyloric sphincter is open (t = 31 s), m/s.

After the pyloric sphincter closes, a residual flow is observed in the intestines at its velocity being about 0.007 m/s ($t = 35$ s) and the flow velocity in the antrum goes down to 0.012 m/s due to lesser amplitude of a peristaltic wave (Fig. 9). Besides, we can observe a circulating flow occurring between peaks of neighboring waves.

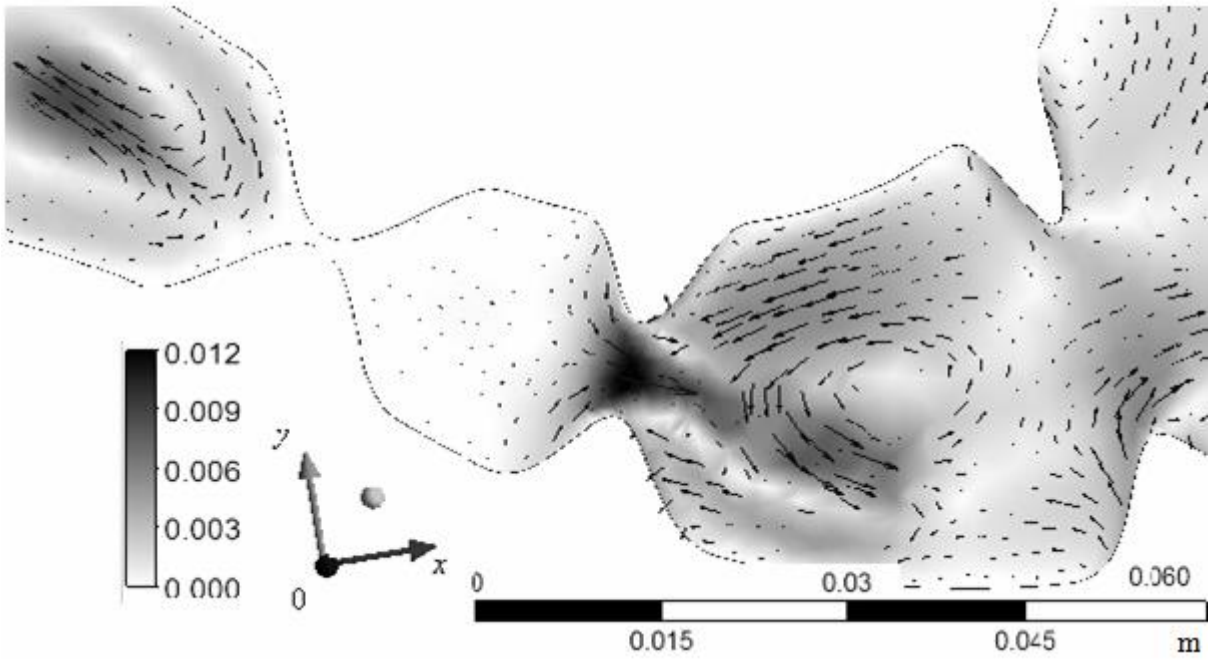

Fig. 9. The velocity field in the antroduodenal section of the stomach after the pyloric sphincter closes (t = 35 s), m/s.

In the second scenario, the stomach functionality $F(t) = const = 0.5$; the peristaltic wave amplitude is assumed to reach 0.0055 m in the antrum. When the pyloric sphincter is closed, the flow profile is similar to the first scenario without any functional disorders but the flow velocity is substantially lower, down to 0.0039 m/s ($t = 28$ s). When the pyloric sphincter is

opened, the stomach contents are evacuated into the intestines at the velocity reaching 0.001 m/s; the flow velocity in the antrum practically does not change and reaches 0.0041 m/s ($t = 31$ s). After the pyloric sphincter closes, a residual flow is observed in the intestines at the velocity being about 0.001 m/s ($t = 35$ s), and the flow velocity in the antrum goes down to 0.0032 m/s. Functional disorders of the stomach motility lead to a substantial decrease in flow velocities (by one order under the stated conditions) and insufficient mixing of the stomach contents.

In the third scenario, a two-phase flow is considered. The first phase is water ($\rho_1 = 1000$ kg/m^3; $\eta_1 = 10^{-3}$ Pa·s) and the second phase is liquid food particles with higher density ($\rho_2 = 1040$ kg/m^3; $\eta_2 = 10^{-3}$ Pa·s). The particles diameter is 0.0008 m, the stomach functionality $F(t) = const = 0.5$, the second phase particles are evenly distributed over the whole modeling area at the initial moment of time (their volume fraction is 10 %). The second phase particles, due to their higher density, rapidly deposit near to the greater curvature of the stomach; two phase are practically divided (Fig. 10). When the pyloric sphincter is closed, a flow zone occurs with the velocity of the first phase reaching 0.0039 m/s ($t = 28$ s). The direction of flow is opposite to the direction of propagation of peristaltic waves. The areas of circulating flows are much less pronounced.

When the pyloric sphincter opens, the first phase is evacuated into the intestines at the velocity reaching 0.002 m/s; the flow velocity in the antrum is about 0.0044 m/s ($t = 31$ s). After the pyloric sphincter closes, a residual flow is observed in the intestines at the velocity being about 0.001 m/s ($t = 35$ s) and the flow velocity in the antrum goes down to 0.0034 m/s (Fig. 11).

Changes in the flow profile in comparison with the one-phase scenario are due to a decrease of the sectional area between wave peaks since the second phase particles act as a peculiar barrier. Circulation of the second phase particles is accomplished when a peristaltic wave goes along the greater curvature of the stomach within the deposition area and the particles are not evacuated under the stated parameters.

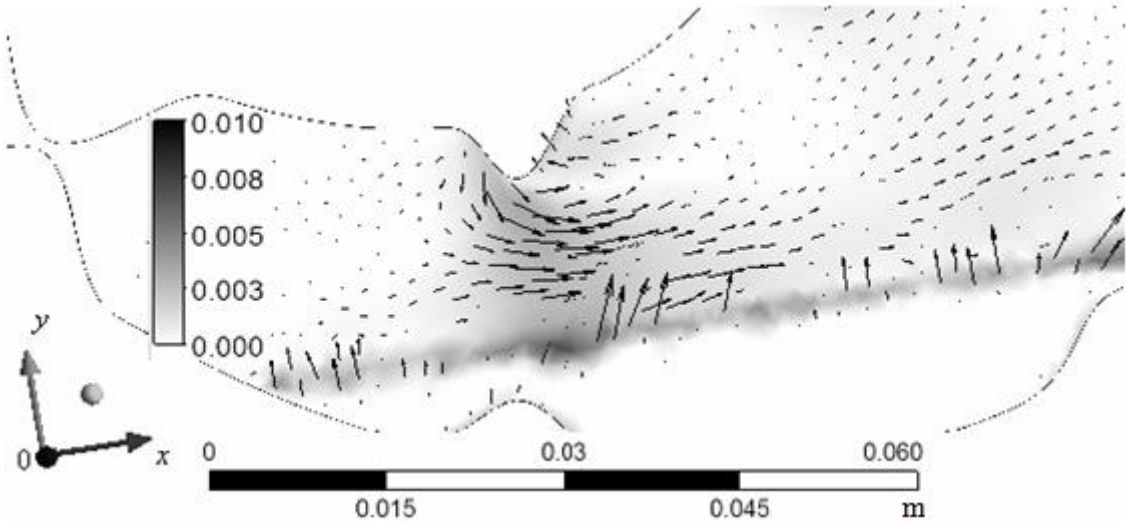

Fig. 10. The velocity field of the first phase in the antrum when the pyloric sphincter is closed (t = 28 s), m/s; the white area adjoining the greater curvature corresponds to the second phase.

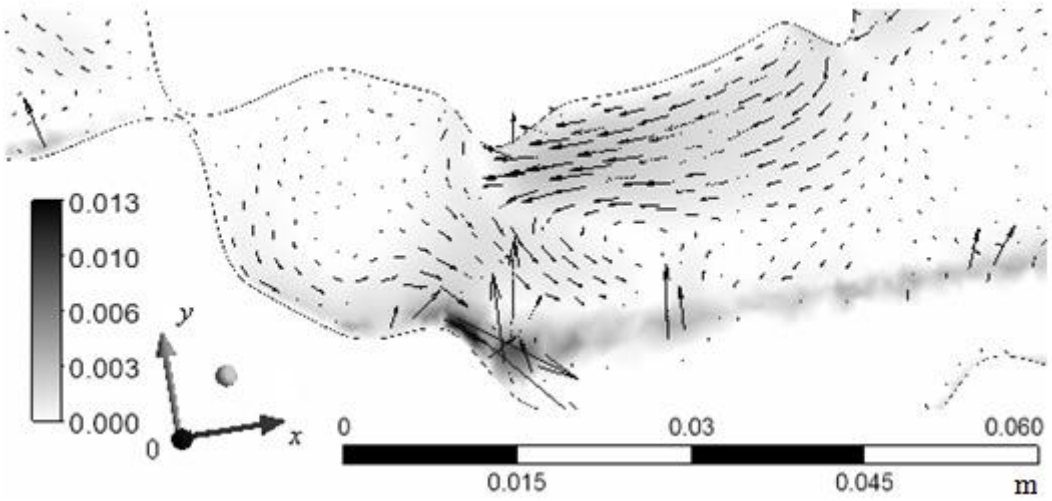

Fig. 11. The velocity field of the first phase in the antroduodenal section of the stomach after the pyloric sphincter closes (t = 31 s), m/s.

Therefore, functional disorders of the antrum motility can have significant influence on intensity of food mixing and the velocity at which the stomach contents are evacuated into the intestines. Although the pyloric area motility has only weak influence on the flow in the antrum, it is important to identify composition and quantity of food entering the intestines for correct modeling of the digestive systems at the meso-level. In future, we plan to accomplish a series of computations considering functional disorders of the pyloric opening motility and disrupted periodicity of the wave process.

CONCLUSION

Therefore, we have developed an algorithm within the meso-level model of the digestive system. The algorithm has been used to create an evolving three-dimensional shape of the GIT antroduodenal area; it is based on the results of individual ultrasound scanning. In future, it seems advisable to adapt the algorithm for mass statistical computations by introducing parameters that change the stomach shape depending on its peculiar structure, type, size, etc.

To specify properties of contraction waves in the antrum and the pyloric sphincter motility, we have created an algorithm for identifying changes in the locations of the computation mesh nodes. A possible way to make the algorithm more complex is introducing the wave process as a multi-stage one and considering modification of the law of wave motion depending on chemical and physical structure of stomach contents (feedback).

We have computed characteristics of a one/two phase medium flow in the GIT antroduodenal section considering the pyloric sphincter motility and functional disorders of the stomach. It is noteworthy that at present only a very limited number of three-dimensional models describing flows in the GIT provide such wide opportunities for research, that is, for analyzing a flow of a multi-phase mixture consisting of various numbers of phases with different viscosity and density. Besides, sizes of food particles may be varied considering dissolution and biochemical reactions; we can also investigate how a body posture influences a flow of a multi-phase mixture. When developing research in this area, we can face certain difficulties due to a limited number of available experimental studies necessary to identify models that are more complex. In addition, model development requires greater computational capacities and multiple statistical calculations call for parallel computing and use of multi-processor systems.

Further development of the meso-level stomach submodel involves considering digestive juice secretion and elements of neuro-endocrine regulation. A priority task is to consider chemical absorption into the circulatory system in the model since identification of chemical

levels in the GIT and blood is necessary for predicting functional disorders of organs and systems at the macro-level when chemicals are introduced orally with food and drinking water.

The research was granted financial support by the Russian Foundation for Basic Research within the research project No. 12-01-00547-a.

REFERENCES

1. Gompertz B. On the Nature of the Function Expressive of the Law of Human Mortality, and on a New Mode of Determining the Value of Life Contingencies. *Philosophical Transactions of the Royal Society of London.* 1825. V. 115. P. 513–585. doi: 10.1098/rstl.1825.0026
2. Makeham W.M. On the Law of Mortality and the Construction of Annuity Tables. *J. Inst. Actuaries.* 1860. V. 8. P. 301–310.
3. Weibull W. A statistical distribution function of wide applicability. *J. Appl. Mech.-Trans.* 1951. V. 18. P. 293–297.
4. Gavrilov L.A., Gavrilova N.S. The reliability theory of aging and longevity. *Journal of Theoretical Biology*. 2001. V. 213. P. 527–545. doi: 10.1006/jtbi.2001.2430
5. Gavrilov L.A., Gavrilova N.S. Models of Systems Failure in Aging. In: *Handbook of Models for Human Aging*. Ed. Conn P.M. Burlington, MA: Elsevier Academic Press; 2006. P. 45–68. doi: 10.1016/B978-012369391-4/50006-0
6. Zueva L.P., Yafaev R.Kh. *Epidemiology. Manual*. Sankt-Petersburg: Foliant Publishers; 2005. (in Russ.).
7. Korotaev A.V., Malkov A.S., Khalturina D.A. *Laws of History: Mathematical Modeling of Historical Macro Processes: Demography, Economy, Wars*. Moscow; 2005. 344 p. (in Russ.).
8. Novosel'tsev V.N. Modeling of the natural technologies of an organism for investigating processes for the control of the organism's vital activities. *Automation and Remote Control*. 1992. V. 53. No. 12. P. 1905–1913.
9. Novosel'tsev V.N. *Fundamental'nye issledovaniia* (Fundamental Research). 2008. No. 6. P. 71-73 (in Russ.).
10. Paltsev M.A., Kvetnoy I.M., Polyakova V.O., Kvetnaiya T.V., Trofimov A.V. Neuroimmunoendocrine mechanisms of aging. *Advances in Gerontology*. 2011. V. 1. No. 1. P. 28–38. doi: 10.1134/S2079057011010103
11. Khavinson V.Kh., Anisimov V.N. 35-year experience in research of peptide regulation of aging. *Advances in Gerontology*. 2009. V. 22. No. 1. P. 11–23 (in Russ.). doi: 10.1007/s10517-009-0650-8
12. Sakovich V.A., Gogoleva M.V., Red'ko V.I., Gubin A.T. Radiation risk load model and its modifications. *Issues of Risk Analysis*. 2004. V. 1. No. 1. P. 76–98 (in Russ.).
13. Mashintsov E.A., Iakovlev A.E. *Izvestiia TulGU. Ser. Matematika. Mekhanika. Informatika* (Proceedings of Tula State University. Series: Mathematics, Mechanics, Information). 2004. V. 10. No. 4. P. 138–174 (in Russ.).
14. Iakovlev A.E. *Matematicheskoe modelirovanie zdorov'ia naseleniia s ispol'zovaniem geoinformatsionnykh tekhnologii* (Mathematical modeling of population health by using geoinformatics technologies): PhD Thesis (Technical Sciences). Tula; 2005. 125 p. (in Russ.).
15. Zaitseva N.V., Trusov P.V., Shur P.Z., Kiryanov D.A., Chigvintsev V.M., Tsinker M.Yu. Mathematical approaches to the health risk assessment of heterogeneous environmental factors based on evolutionary models. *Health Risk Analysis*. 2013. No. 1. P. 3–11 (in Russ.).
16. Trusov P.V., Zaitseva N.V., Kiryanov D.A., Kamaltdinov M.R., Cinker M.Ju., Chigvintsev V.M., Lanin D.V. A Mathematical Model for Evolution of Human

Functional Disorders Influenced by Environment Factors. *Mathematical Biology and Bioinformatics*. 2012. V. 7. No. 2. P. 589–610 (in Russ.). doi: 10.17537/2012.7.589

17. Zaitseva N.V., Kiryanov D.A., Lanin D.V., Chigvintsev V.M. A mathematical model of the immune and neuroendocrine systems mutual regulation under the technogenic chemical factors impact. *Computational and Mathematical Methods in Medicine*. 2014. V. 2014. Article ID 492489. doi: 10.1155/2014/492489
18. Feinle C., Kunz P., Boesiger P., Fried M., Schwizer W. Scintigraphic validation of a magnetic resonance imaging method to study gastric emptying of a solid meal in human. *Gut*. 1999. V. 44. P. 106–111. doi: 10.1136/gut.44.1.106
19. Marciani L., Gowland P.A., Spiller R.C., Manoj P., Moore J.R., Young P., Al-Sahab S., Bush D., Wright J., Fillery-Travis A.J. Gastric response to increased meal viscosity assessed by echo-planar magnetic resonance imaging in humans. *The journal of nutrition*. 2000. V. 130. P. 122–127.
20. Jones K.L., O'Donovan D.G., Horowitz M., Russo A., Lei Y., Hausken T. Effects of posture on gastric emptying, transpyloric flow, and hunger after a glucose drink in healthy humans. *Dig. Dis. Sci*. 2006. V. 51. P. 1331–1338. doi: 10.1007/s10620-005-9010-3
21. Simonian H.P., Maurer A.H., Knight L.C., Kantor S., Kontos D., Megalooikonomou V., Fisher R.S., Parkman H.P. Simultaneous assessment of gastric accommodation and emptying: studies with liquid and solid meals. *J. Nucl. Med*. 2004. V. 45. P. 1155–1160.
22. Liao D., Gregersen H., Hausken T., Gilja O.H., Mundt M., Kassab G. Analysis of surface geometry of the human stomach using real-time 3-D ultrasonography *in vivo*. *Neurogastroenterol Motil*. 2004. V. 16. P. 315–324. doi: 10.1111/j.1365-2982.2004.00522.x
23. Frokjaer J.B., Andersen S.D., Drewes A.M., Gregersen H. Ultrasound-determined geometric and biomechanical properties of the human duodenum. *Dig. Dis. Sci*. 2006. V. 51. P. 1662–1669. doi: 10.1007/s10620-005-9015-y
24. Karasikov N.V., Mikheev A.G., Mishulin L.E., Rakitin B.V., Trifonov M.M., Schookin S.I. Gastrointensinal manometry with medical device "Gastroscan-D". *Biomedical Radio Electronics*. 2011. No. 10. P. 79–83 (in Russ.).
25. Chernyakevich S.A. Motor function of upper sections of digestive system in norm and pathology. *Russian Journal of Gastroenterology, Hepatology, Coloproctology*. 1998. No. 2. P. 33–39 (in Russ.).
26. De Schepper H.U., Cremonini F., Chitkara D., Camilleri M. Assessment of gastric accommodation: overview and evaluation of current methods. *Neurogastroenterol. Motil*. 2004. V. 16. P. 275–285. doi: 10.1111/j.1365-2982.2004.00497.x
27. Kornienko E.A., Dmitrienko M.A., Nikulin Iu.A., Filiushkina E.I., Filiushkin I.P. *Primenenie meditsinskoi tekhniki pri funktsional'noi diagnostike v gastroenterologii. Uchebno-metodicheskoe posobie* (Using Medical Equipment in Gastroenterological Diagnostics. Handbook). Sankt-Petersburg; 2006. 103 p. (in Russ.).
28. Stupin V.A., Smirnova G.O., Baglaenko M.V., Siluyanov S.V., Zakirov D.B. Peripheral electrogastroenterography in the diagnosis of disorders of motor-evacuation function of the gastrointestinal tract. *Lechashchy Vrach (The Practitioner)*. 2005. No. 2. P. 60–62 (in Russ.).
29. Smirnova G.O., Siluyanov S.V. *Peripheral Electrogastroenterography in Clinical Practice*. Ed. V.A. Stupin. Moscow; 2009. 20 p. (in Russ.).
30. Rapoport S.I., Lakshin A.A., Rakitin B.V., Trifonov M.M. *pH metry of the esophagus and stomach in the upper digestive tract diseases*. Ed. F.I. Komarov. Moscow: Medpraktika-M; 2005. 208 p. (in Russ.).
31. Sotnikov V.N., Dubinskaia T.K., Volova A.V., Iakovlev G.A. *Znachenie endoskopicheskoi pH-metrii v opredelenii kislotoprodutsiruiushchei funktsii zheludka. Posobie dlia vrachei* (The Role of Endoscopic pH metry in Estimation of the Acid-

forming Function of the Stomach. Physician Handbook). Moscow; 2005. 35 p. (in Russ.).
32. Oomen A.G., Rompelberg C.J.M., Bruil M.A., Dobbe C.J.G., Pereboom D.P.K.H., Sips A.J.A.M. Development of an in vitro digestion model for estimating the bioaccessibility of soil contaminants. *Archives of environmental contamination and toxicology*. 2003. V. 44. P. 281–287. doi: 10.1007/s00244-002-1278-0
33. Arnold J.G., Dubois A. In vitro studies of intragastric digestion. *Digestive disease and sciences*. 1983. V. 28. P. 737–741. doi: 10.1007/BF01312565
34. Hedren E., Diaz V., Svanberg U. Estimation of carotenoid accessibility from carrots determined by an *in vitro* digestion method. *European Journal of clinical Nutrition*. 2002. V. 56. P. 425–430. doi: 10.1038/sj.ejcn.1601329
35. Hedren E., Diaz V., Svanberg U. Estimation of carotenoid accessibility from carrots determined by an *in vitro* digestion method. *European Journal of clinical Nutrition*. 2002. V. 56. P. 425–430. doi: 10.1038/sj.ejcn.1601329
36. Nagah A.M., Seal C.J. *In vitro* procedure to predict apparent antioxidant release from wholegrain foods measured using three different analytical methods. *Journal of the science of food and agriculture*. 2005. V. 85. P. 1177–1185. doi: 10.1002/jsfa.2106
37. Walsh K.R., Zhang Y.C., Vodovitz Y., Schwartz S.J., Failla M.L. Stability and bioaccessibility of isoflavones from soy bread during *in vitro* digestion. *Journal of agricultural and food chemistry*. 2003. V. 51. P. 4603–4609. doi: 10.1021/jf0342627
38. Molly K., Woestyne M.V., Verstraete W. Development of a 5-step multi-chamber reactor as a simulation of the human intestinal microbial ecosystem. *Appl. Microbiol. Biotechnol*. 1993. V. 39. P. 254–258. doi: 10.1007/BF00228615
39. Cardot J.-M., Beyssac E., Alric M. *In vitro-in vivo* correlation: importance of dissolution in IVIVC. *Dissolution technologies*. 2007. V. 14. P. 15–19. doi: 10.14227/DT140107P15
40. Kong F., Singh R.P. Modes of disintegration of solid foods in simulated gastric environment. *Food biophysics*. 2009. V. 4. P. 180–190. doi:10.1007/s11483-009-9116-9
41. Kong F., Singh R.P. Solid loss of carrots during simulated gastric digestion. *Food biophysics*. 2011. V. 6. P. 84–93. doi: 10.1007/s11483-010-9178-8
42. Schulze K. Imaging and modeling of digestion in the stomach and the duodenum. *Neurogastroenterol. Motil*. 2006. V. 18. P. 172–183. doi: 10.1111/j.1365-2982.2006.00759.x
43. Samura B.A., Dralkin A.V. *Farmakokinetika* (Pharmacokinetika). Khar'kov; 1996. 286 p. (in Russ.).
44. Colov'ev V.H., Firsov A.A., Filov V.A. *Farmakokinetika* (Pharmacokinetika). Moscow; 1980. 432 p. (in Russ.).
45. Ferrua M.J, Singh R.P. Modeling the fluid dynamics in a human stomach to gain insight of food digestion. *Journal of food science*. 2010. V. 75. P. 151–162. doi: 10.1111/j.1750-3841.2010.01748.x
46. Singh S., Singh R.P. Gastric Digestion of Foods: Mathematical Modeling of Flow Field in a Human Stomach. *Food Engineering Interfaces*. 2011. P. 99–117.
47. Xue Z., Ferrua M.J., Singh R.P. Computational fluid dynamics modeling of granular flow in human stomach. *Alimentos hoy*. 2012. V. 21. P. 3–14.
48. Dillard S., Krishnan S., Udaykumar H.S. Mechanics of flow and mixing at antroduodenal junction. *World J. Gastroenterol*. 2007. V. 13. P. 1365–1371. doi: 10.3748/wjg.v13.i9.1365
49. Kozu H., Kobayashi I., Nakajima M., Uemura K., Sato S., Ichikawa S. Analysis of flow phenomena in gastric contents induced by human gastric peristalsis using CFD. *Food Biophysics*. 2010. V. 5. P. 330–336. doi: 10.1007/s11483-010-9183-y
50. Kong F., Singh R.P. Disintegration of solid foods in human stomach. *Journal of food science*. 2008. V. 73. P. 67–80. doi: 10.1111/j.1750-3841.2008.00766.x

51. Pal A., Indireshkumar K., Schwizer W., Abrahamsson B., Fried M., Brasseur J.G. Gastric flow and mixing studied using computer simulation. *Proc. R. Soc. Lond. B*. 2004. V. 271. P. 2587–2594. doi: 10.1098/rspb.2004.2886
52. Pal A., Brasseur J.G, Abrahamsson B. A stomach road or “Magenstrasse” for gastric emptying. *Journal of Biomechanics*. 2007. V. 40. P. 1202–1210. doi: 10.1016/j.jbiomech.2006.06.006
53. Trusov P.V., Zaytseva N.V., Kamaltdinov M.R. Simulation of digestion processes in consideration of functional disorders in a human organism: conceptual and mathematical formulations, model structure. *Russian Journal of Biomechanics*. 2013. V. 17. No. 4. P. 60–74.
54. Nigmatulin R.I. *Dynamics of Multiphase Media*. Vol. 1. Hemisphere, Washington; 1991.
55. Schiller L., Naumann Z. A drag coefficient correlation. *Ver. Deutsh. Ing*. 1935. V. 77. P. 318.
56. Barequet G., Shapiro D., Tal A. Multilevel sensitive reconstruction of polyhedral surfaces from parallel slices. *The Visual Computer*. 2000. V. 16. P. 116–133. doi: 10.1007/s003710050201
57. Lobregt S., Viergever A. A discrete dynamic contour model. *IEEE transactions on medical imaging*. 1995. V. 14. P. 12–24. doi: 10.1109/42.370398
58. Nedzvezd A., Lukashevich P., Ablameyko S., Deserno T. M., Lehmann. Reconstruction of 3D medical object shapes from 2D cross-sections. In: *Pattern recognition and information processing*: proceedings of the tenth international conference. Eds. Krasnoproshin V., Ablameyko S., Sadykhov R. 2009. P. 247–250.
59. Rohling R.N. *3D Freehand Ultrasound: Reconstruction and Spatial Compounding*: PhD Dissertation. University of Cambridge; 1998. P. 158.
60. Treece G.M. *Volume Measurement and Surface Visualisation in Sequential Freehand 3d Ultrasound*: PhD Dissertation. University of Cambridge; 2000. P. 172.
61. *Ansys fluent 12.0. Theory guide*. 2009.

Received 19.05.2023.
Published 05.09.2023.